

Nonadiabatic quantum pumping in mesoscopic nanostructures

C. S. Tang¹ and C. S. Chu²

¹*Physics Division, National Center for Theoretical Sciences, P.O. Box 2-131, Hsinchu 30013, Taiwan*

²*Department of Electrophysics, National Chiao Tung University, Hsinchu 30010, Taiwan*

We consider a nonadiabatic quantum pumping phenomena in a ballistic narrow constriction. The pumping is induced by a potential that has both spatial and temporal periodicity characterized by K and Ω . In the zero frequency ($\Omega = 0$) limit, the transmission through narrow constriction exhibits valley structures due to the opening up of energy gaps in the pumping region — a consequence of the K periodicity. These valley structures remain robust in the regime of finite Ω , while their energies of occurrence are shifted by about $\hbar\Omega/2$. The direction of these energy shifts depend on the directions of both the phase-velocity of the pumping potential and the transmitting electrons. This frequency dependent feature of the valley structures gives rise to both the asymmetry in the transmission coefficients and the pumping current. An experimental setup is suggested for a possible observation of our nonadiabatic quantum pumping findings.

PACS numbers: 73.23.-b, 73.23.Ad, 73.50.Mx, 72.10.-d

The phenomenon of adiabatic quantum pumping in mesoscopic systems has attracted much attention since the first proposal by Thouless [1]. The pumping phenomena refer to net transport of charges at zero bias. Mechanisms giving rise to quantum pumping involves cyclic deformations of more than one parameter in the system. The adiabatic deformation causes the transmission of a finite amount of charges in one deformation cycle. For the cases when this finite charge transfer is quantized the pumping could be of importance in establishing a standard of electric current [2]. The first experimental demonstration of the pumping of charges was reported by Switkes *et al.* [3]. They applied sinusoidal voltages to two metal gates that define the shape of an open quantum dot. The phase difference between the two metal gates is an important adjustable parameter for the pumping of charges. Subsequent theoretical studies on this pumping mechanism in quantum dots have invoked a double oscillating barrier model [4, 5]. More recently, it was pointed out that quantum interference also plays an important role in the pumping of charges [6]. Thus far, most of the studies have concentrated on the adiabatic regime [7]. It is legitimate then to explore the nonadiabatic aspect of the pumping phenomena.

In this work, our purposes are threefold: to treat the pumping phenomena nonadiabatically, to analyze in detail a novel pumping mechanism found in our results, and to propose an experimental setup for a possible realization of the mechanism. Towards these ends, we have implemented a generalized scattering-matrix method that allows us to solve the time-dependent Schrödinger equation to effectively all orders in the pumping potential [8]. Hence our results are not limited by the adiabatic approximation. Furthermore, in analyzing our results more closely, we are able to identify a pumping mechanism that is associated with coherent inelastic scatterings of the transmitting electron in the pumping region. That the above quantum transitions play a decisive role in this

pumping phenomena shows the nonadiabatic nature of the phenomena. We stress that this pumping phenomena do not require an asymmetry in the system configuration. The phase velocity of the pumping potential alone is sufficient to cause the pumping.

The pumping potential $V(x, t)$ we invoked acts upon a certain region of a ballistic narrow channel. Apart from the overall spatial envelope of the potential, $V(x, t)$ is periodic in time t , with a period $T = 2\pi/\Omega$, and periodic along the longitudinal location x , with a period $L_p = 2\pi/K$. We assume a simple envelope profile for the potential,

$$V(x, t) = V_0 \cos(Kx - \Omega t) \Theta(L/2 - |x|), \quad (1)$$

expecting it to have captured the essential physics of the pumping mechanism. Within the pumping region, the pumping potential has a phase velocity $v = \Omega/K$, right-going in this case, and the longitudinal dimension it covered is L . As long as $L \gg L_p$, the detail form of the envelope profile — such as a less abrupt profile — should not change the pumping features found in this work. Meanwhile, similar potential form has been considered by O. Entin-Wohlman *et al.* [9] in their study on the acoustoelectric effect in a finite-length ballistic quantum channel. The potential was generated from the surface acoustic wave, and was assumed to be significant only inside the channel while it was totally screened in the terminals. Even though the potential we consider in this work is of similar form to that of theirs, the physical regimes of interest are different. They considered the regime that incoherent processes occur frequent enough in the channel to sustain a well defined local distribution of the electrons [9].

Our interest, however, is in the coherent regime: that electrons traversing the channel can maintain their phase coherence without encountering any incoherent processes. It turns out that the incoherent and the coherent regimes exhibit different transport characteristics.

For instance, in the incoherent regime, the pumping feature was found to be most significant only in the vicinity of the subband threshold [9], whereas in the coherent regime, we find significant pumping features in the conductance plateau regions.

To simplify our presentation, we choose the energy unit $E^* = E_F$, the length unit $a^* = 1/k_F$, the time unit $t^* = \hbar/E^*$, and the frequency unit $\Omega^* = 1/t^*$. Here E_F and k_F represent, respectively, the Fermi energy and the Fermi wave vector in the reservoirs. The Hamiltonian is of the form $\hat{H} = \hat{H}_y + \hat{H}_x(t)$, where $\hat{H}_y = -\partial^2/\partial y^2 + \omega_y^2 y^2$ contains a transverse confinement, leading to transverse subbands with energy levels $\varepsilon_n = (2n+1)\omega_y$ and a subband level spacing $\Delta\varepsilon = 2\omega_y$. The time-dependent and the longitudinal part of the Hamiltonian $\hat{H}_x(t)$ is of the form $\hat{H}_x(t) = -\partial^2/\partial x^2 + V(x, t)$.

At zero source-drain bias, the chemical potential μ is the same in the reservoirs that connect to the two ends of the constriction. The pumped current consists of contribution from all electrons, given by

$$I = -\frac{2e}{h} \int_0^\infty dE f(E - \mu) [T_{\rightarrow}(E) - T_{\leftarrow}(E)]. \quad (2)$$

Here $f(E - \mu)$ is the Fermi distribution function and $-e$ is the charge of an electron. In addition, T_{\rightarrow} and T_{\leftarrow} are, respectively, the total current transmission coefficients for the right- and left-going incident electrons and for a given incident energy E . Contributions from all sidebands, denoted by m , and all subbands, denoted by n , have been taken into account, given by

$$T_{\rightarrow(\leftarrow)}(E) = \sum_n \sum'_m T_{n \rightarrow(\leftarrow)}^m, \quad (3)$$

where the primed summation includes only propagating components of the transmitted electrons. The $T_{n \rightarrow(\leftarrow)}^m$ denote the transmission coefficients for the processes that an incident electron in subband n , energy E , passes through the pumping region and ends up in energy $E + m\Omega$ on the other end of the constriction. These coefficients are solved by a generalized scattering-matrix method that we had established to treat time-dependent scattering potential nonperturbatively [10]. We had applied this method to cases of longitudinally polarized field [11] and transversely polarized field [12]. Essentially, in this method, we segmented the scattering potential along the longitudinal direction into slices, solved the scattering matrix of each slice, and constructed the total scattering matrix [8]. The energy derivative of the pumped current $\partial I/\partial\mu$ is given, in the low temperature limit, by

$$\frac{\partial I}{\partial\mu} = -\frac{2e}{h} [T_{\rightarrow}(\mu) - T_{\leftarrow}(\mu)]. \quad (4)$$

In our numerical examples, we present the μ dependencies of the current transmission coefficients and $\partial I/\partial\mu$.

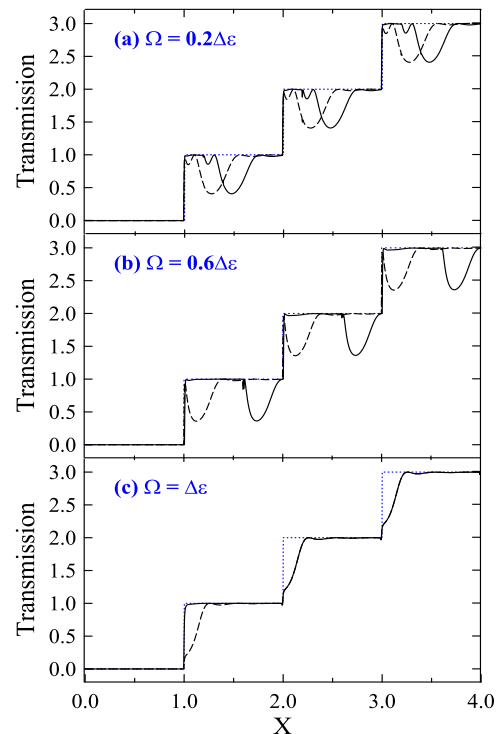


FIG. 1: The current transmission coefficient as a function of X for $\Omega/\Delta\varepsilon = 0.2, 0.6$, and 1.0 in Figs. 1(a)-1(c), respectively. Other parameters are $K = 0.15$, and $L = 150$. Solid curves and dashed curves are the transmissions of the right- and left-going incident electrons, respectively, and for $V_0 = 0.002$. Dotted curves are for $V_0 = 0.0$.

The values of the parameters used are consistent with that for a typical high mobility two-dimensional electron gas formed at a GaAs - $\text{Al}_x\text{Ga}_{1-x}\text{As}$ heterostructure, with $E^* = 9$ meV, $a^* = 1/k_F = 79.6$ Å, and $\Omega^* = E^*/\hbar = 13.6$ Trad/s. We also choose $\omega_y = 0.007$ such that the subband energy-level spacing $\Delta\varepsilon = 0.014$ ($\simeq 0.126$ meV). For the pumping potential, we chose $V_0 = 0.002$, $K = 0.15$, and the longitudinal range $L = 150$ such that $KL/2\pi \simeq 3.58$. The chemical potential μ is replaced by

$$X = \frac{\mu}{\Delta\varepsilon} + \frac{1}{2},$$

where the integral value of X stands for the number of propagating subbands in the constriction. The dependence of the current transmission coefficients T_{\rightarrow} and T_{\leftarrow} on X are depicted by the solid and the dashed curves in Fig. 1, respectively. The dotted curves are for $V_0 = 0$ and angular frequency Ω equals $0.2\Delta\varepsilon$, $0.6\Delta\varepsilon$, and $\Delta\varepsilon$, respectively, in Figs. 1(a)-(c).

The general features presented in Fig. 1 are summarized in the following. In the absence of the pumping potential, the transmission coefficients T_{\rightarrow} and T_{\leftarrow} exhibit the well understood quantized features, reflecting the number of propagating subbands in the constrictions.

That both of the transmission coefficients are given by the same dotted curve reflects the symmetry in the transmission of the electrons with respect to their incident directions. This symmetry, however, is broken by the introduction of pumping potentials to the constriction. Upon the action of the pumping potential, a valley structure is developed in each of the plateau regions, but the energies of occurrence for these valley structures are different for T_{\rightarrow} and T_{\leftarrow} . A valley structure in Fig. 1 is characterized by a substantial drop in the transmission coefficient, with maximum drop $|\Delta T_{\max}| > 0.5$, and a large energy width, with $\Delta X_{\text{valley}} \approx 0.4\Delta\varepsilon$. Valley structures for T_{\leftarrow} occur at lower energies than that for T_{\rightarrow} on the same plateau. Interestingly, the separation in energy, or ΔX , between the minimums of the valley structures and belonging to the same plateau for T_{\rightarrow} and T_{\leftarrow} , increases with the angular frequency Ω of the pumping potential. In fact, our numerical results show that $\Delta X = \Omega/\Delta\varepsilon$. For the case when $\Omega = \Delta\varepsilon$, the separation becomes so large that the T_{\rightarrow} valley structures overlap with the T_{\leftarrow} valley structures of the next higher subbands. These valley structures and the asymmetry in the transmission coefficients are the key results in this work.

We note in passing that there are small oscillatory structures in Fig. 1(a) in the energy range between the subband threshold and the valley structure. These harmonic structures are associated with multiple scatterings of the transmitting electrons in between the two edges of the pumping potential.

Before we present a physical explanation for the valley structures, we want to make one more remark: all the valley structures in Figs. 1(a) and 1(b) are almost identical in their profile regardless of their differences in the energies of occurrence and the incident direction of the electrons. Furthermore, even though the valley structures in Fig. 1(c) are truncated at the threshold energies, the remaining profile compares well with those in Figs. 1(a) and 1(b). These Ω -independent features prompted us to check the $\Omega = 0$ case, and we find indeed the same valley structure profiles except that the transmission symmetry is restored, with both T_{\rightarrow} and T_{\leftarrow} curves falling on top of one another. This $\Omega = 0$ result is not presented here, but we learn from this result that the energies of occurrence for the finite Ω valley structures of T_{\rightarrow} and T_{\leftarrow} have been shifted by about $\Omega/2$ and $-\Omega/2$, respectively, from their $\Omega = 0$ counterparts. The $\Omega = 0$ valley structures are certainly associated with the formation of an energy band gap inside the region acted upon by the potential $V(x)$. It is conceivable then that the valley structures in the finite Ω regime are caused by the establishment of a resonant coupling between some *degenerate* states via the pumping potential. To drive this point home and to obtain an analytic expression for the energies of occurrence of the valley structures, we propose a two-component approximation for the wavefunction along the constriction,

given by

$$\begin{aligned} \psi(x,t) = & \exp(ikx - iEt) \\ & + C \exp[i(k-K)x - i(E-\Omega)t]. \end{aligned} \quad (5)$$

The above wavefunction has taken up a near resonance approximation that describes the resonant coupling of an electron with photons. Substituting Eq. (5) into a 1D Schrödinger equation

$$[-\partial^2/\partial x^2 + V_0 \cos(Kx - \Omega t)] \psi(x,t) = i\partial/\partial t \psi(x,t),$$

and retaining only terms of the form as in $\psi(x,t)$, we obtain

$$E = \frac{1}{2} \left[\Omega + \varepsilon_k + \varepsilon_{k-K} \pm \sqrt{(\Omega + \varepsilon_{k-K} - \varepsilon_k)^2 + V_0^2} \right], \quad (6)$$

where E is the energy spectrum of an electron coupled with photons in the system, and $\varepsilon_k = k^2$.

The energy spectrum has an energy gap at the resonant coupling condition given by $\varepsilon_k = \varepsilon_{k-K} \pm \Omega$. The plus, and minus, sign in the resonant coupling condition is for positive, and negative, k , respectively. This in turn corresponds to right- and left-going states. The 1D kinetic energy ε_k at the center of the energy gap is $\varepsilon_{\text{Gap}} = [(K/2)(1 \pm \Omega/K^2)]^2$, which can be approximated by $K^2/4 \pm \Omega/2$ when $\Omega \ll K^2$. In the case for a constriction, the energies of occurrence will be at $X_{\text{Gap}} = N + \varepsilon_{\text{Gap}}/\Delta\varepsilon$. These X_{Gap} 's correspond to the minimums of the valley structures in Figs. 1(a)-(c). More specifically, in Fig. 1(a), $X_{\text{Gap}} = 1.51, 2.51, 3.51$ for the right-going electrons, and $X_{\text{Gap}} = 1.31, 2.31, 3.31$ for the left-going electrons. The matches of these values with the minimums of the valley structures are remarkable.

Besides the energies of occurrence, Eq. (6) also provides us an estimate for the energy gap, given by $\Delta X_{\text{Gap}} = V_0/\Delta\varepsilon = 0.143$ for our case. This ΔX_{Gap} is less than $\Delta X_{\text{valley}} \approx 0.4$, the width of the valley structures in Fig. 1. We have tried other cases of longer L and find out that ΔX_{valley} decreases with increasing L . Its value becomes 0.2 at $L = 400$. In addition, the maximum drop in the transmission coefficient $|\Delta T_{\max}|$ for the valley structures is very close to unity when $L = 400$. Thus we conclude that the seeming discrepancy between ΔX_{Gap} and ΔX_{valley} in Fig. 1 is resulted from the finite L effect. The detail profile of the transmission coefficients, however, is given by our nonperturbative approach.

We have shown that the valley structures in the finite Ω regime are resulted from the coherent inelastic scatterings in the pumping region. The Ω -dependence in the energies of occurrence X_{Gap} reflects the breaking of the transmission symmetry by the phase velocity of the pumping potential.

In Fig. 2, we present the effects of the transmission asymmetry on the quantum pumping by plotting $\partial I/\partial \mu$ as a function of X . The parameters are the same as those

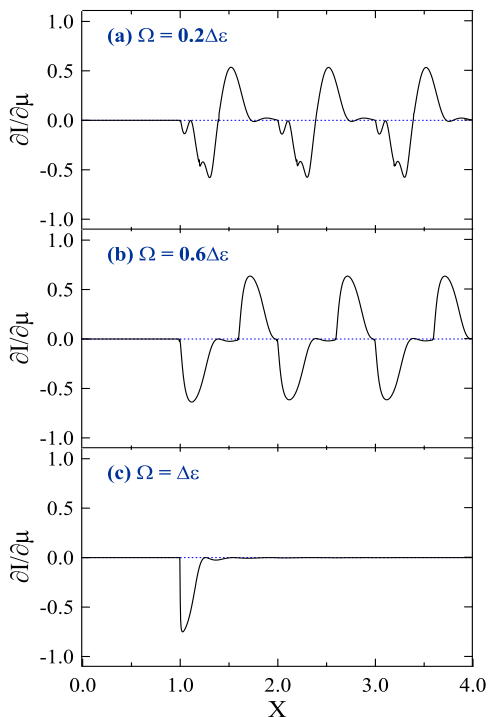


FIG. 2: The energy derivative of the pumped currents, in units of $2e/h$, as a function of X for $\Omega/\Delta\varepsilon = 0.2, 0.6$, and 1.0 in Figs. 2(a)-2(c), respectively. Other parameters are the same as those in Fig. 1. Solid curve is for $V_0 = 0.002$ and dotted curves are for $V_0 = 0.0$.

in Fig. 1. Major features shown in Figs. 2(a), 2(b) are alternate valley and broad peak structures. These are due to suppression in the transmission for electrons incident from the right, and left, electrode, respectively. The valley and the broad peak structures barely resemble each other in Fig. 2(a). However, the corresponding structures in Fig. 2(b) are almost inversion images of one another. Since the valley structures for the two transmission coefficients overlap in Fig. 1(a), their contributions to $\partial I/\partial\mu$ suffer from partial cancellation between themselves. This cancellation hampers the resemblance between the valley and the broad peak structures in Fig. 2(a). On the other hand, the valley structures are well separated in Fig. 1(b), thus preserving the resemblance between the valley and the broad peak structures in Fig. 2(b). The case of exact cancellations is presented in Fig. 2(c), when the valley structures of T_{\rightarrow} overlap with the valley structures of T_{\leftarrow} of the next subbands. Only the first valley structure survives and the net flow of the electrons is in the same direction as the phase velocity of the pumping potential. Finally, we stress that the pumping effect is most significant in the conductance plateau regions. This is in sharp contrast to the pumping effect in the incoherent regime [9].

For the possible realization of the pumping mechanism proposed in this work, we suggest an experimental setup

that has taken full advantage of the recently developed finger gate technology [13, 14]. The basic structure is a narrow constriction defined out of a two dimensional electron gas by a pair of split-gates (SG). On top of this SG, and separated vertically by an insulating layer of submicron thickness, are two interdigitated finger gates (FG) that are oriented transversely. Each of these FGs has a period L_p . The pumping potential could be generated by subjecting the FGs to AC bias of the same frequency while maintaining a phase difference between the two FGs. The control of the phase difference in the bias voltage between two neighboring gates was successfully demonstrated by Switkes *et al* [3] in the $f \approx 10$ MHz region. More recently, phase-shifter operating in the $f \approx 10$ GHz region has been fabricated using a $0.6\text{-}\mu\text{m}$ GaAs process [15]. Hence we believe that the suggested experimental setup, though poses a stringent challenge to the experimentalists, is within reach of the present nanotechnology.

In conclusion, we have proposed and have analyzed in detail a nonadiabatic quantum pumping mechanism. We have demonstrated the robustness of such pumping mechanism due to its resonant coupling nature. And we have proposed an experimental setup for the possible realization of such mechanism.

C.S.T. thanks Professor Y. C. Lee for his enthusiastic encouragement. This work was supported by NSC of the ROC under Contract No. NSC89-2112-M-236-001 and NSC90-2112-M-009-003.

-
- [1] D. J. Thouless, Phys. Rev. B **27**, 6083 (1983).
 - [2] Q. Niu, Phys. Rev. Lett. **64**, 1812 (1990).
 - [3] M. Switkes, C. M. Marcus, K. Campman, and A. C. Gosard, Science **283**, 1905 (1999).
 - [4] M. Wagner, Phys. Rev. Lett. **85**, 174 (2000).
 - [5] Y. Wei, J. Wang, and H. Guo, Phys. Rev. B **62**, 9947 (2000).
 - [6] F. Zhou, B. Spivak, and B. Altshuler, Phys. Rev. Lett. **82**, 608 (1999).
 - [7] C. Liu and Q. Niu, Phys. Rev. B **47**, 13031 (1993). The authors considered the nonadiabatic effect of a monotonically rising barrier on the quantum charge pumping.
 - [8] C. S. Tang and C. S. Chu, Physica B **292**, 127 (2000).
 - [9] O. Entin-Wohlman, Y. Levinson, and Yu. M. Galperin, Phys. Rev. B **62**, 7283 (2000).
 - [10] C. S. Tang and C. S. Chu, Phys. Rev. B **53**, 4838 (1996); Physica B **254**, 178 (1998).
 - [11] C. S. Tang and C. S. Chu, Phys. Rev. B **60**, 1830 (1999).
 - [12] C. S. Chu and C. S. Tang, Solid State Commun. **97**, 119 (1996).
 - [13] C.-T. Liang, M. Y. Simmons, C. G. Smith, G. H. Kim, D. A. Ritchie, and M. Pepper, Phys. Rev. Lett. **81**, 3507 (1998).
 - [14] I. Tralle, Physica E **9**, 275 (2001).
 - [15] F. Ellinger, R. Vogt, and W. Bächtold, IEEE Trans. Microwave Theory Tech. **49**, 913 (2001).